PHYSICAL REVIEW D VOLUME 16, NUMBER 1 1 JULY 1977

Reanalysis of three-pion production data with fully analytic, unitary functions*

R. L. Schult and H. W. Wyld, Jr.
Department of Physics, University of Illinois at Urbana-Champaign, Urbana, Illinois 61801
(Received 7 February 1977; revised manuscript received 4 April 1977)

The angular momentum analysis of the reaction $\pi^- p \to \pi^- \pi^+ \pi^- p$ has been improved by using three-pion-state amplitudes which both satisfy unitarity and have proper analytic structure. The integral equations for these amplitudes and the method of solution used are discussed. The results of fitting the CERN-IHEP data at 25 and 40 GeV/c for $\pi^- p \to \pi^- \pi^+ \pi^- p$ are almost identical to the earlier fits; in particular, the amplitude for the $J^P = 1^+$ state still has no large phase change over the mass region where its magnitude has a maximum (the A_1 bump). We do, however, point out that there are ambiguities in the fit which make the phase determination less clear than earlier reports indicated.

I. INTRODUCTION

Interpretation of the peak at about 1200 MeV in the three-pion mass distribution for the reaction $\pi^- p \to \pi^- \pi^+ \pi^- p$ has been controversial ever since it was first noted (Refs. 1, 2, 3, and earlier works cited therein). On one hand, the peak may be a resonance (the A_1) and, on the other hand, it may only be a kinematic reflection of some other process. The Deck mechanism is a favorite kinematical effect which has been used to try to explain the peak, but it tends to produce too broad a bump.[4] An early proposal, called the Peierls mechanism,[5,6] attempted to explain the peak as due to the one-pion-exchange contribution in $\rho\pi$ scattering. This model was rejected when it was pointed out by Goebel[7] that the one-pion-exchange singularity is on the (unphysical) second Riemann sheet for processes which involve production of the $\rho\pi$ state.

Antipov *et al.*[1,2] and earlier workers attempted to clarify the experimental situation by analyzing the data with Ascoli's isobar-model analysis program FIT, which removes explicitly the two-pion final-state interactions (ρ, ϵ, f mesons) and decomposes the three-pion system according to total angular momentum and parity. For any J^P state in which there is a resonance, the fitting function $C^{JP}(M_{3\pi})$ was expected to have the characteristic Breit-Wigner form $(M_{A_1}^2 - M_{3\pi}^2 - iM_{A_1}\Gamma_{A_1})^{-1}$. This was indeed the case for the 2^+ state (the A_2 resonance); however, the 1^+ state has a bump but no phase change.

The isobar model was criticized[8] on the basis that, because of the symmetrization of the identical pions in the $\pi^-\pi^+\pi^-$ system, the amplitudes used did not satisfy two-body unitarity. This criticism was answered by Ascoli and Wyld,[3] who used a K-matrix formalism to write integral equations for amplitudes which would be unitary. Reanalysis of the data with these functions showed no major changes, but some details were different, in particular the fits were not as good.

This unitarized K-matrix formalism was then criticized[9,10] as having introduced the faults of the Peierls model in that the one-pion-exchange singularity had been brought up to the physical sheet, i.e., that the amplitudes did not have the correct analyticity properties. Several suggestions for generating appropriate amplitudes have been proposed, but the procedure is not unique, and numerical results are just beginning to become available.[11-16]

We have picked one possible procedure which should generate unitary and analytic amplitudes, namely relativistic Faddeev equations similar to those of Mennessier, Pasquier, and Pasquier[17] and Aaron, Amado, and Young.[18] In Sec. II these equations are given and the ambiguous arbitrary two-body input functions used are specified. In Sec. III the numerical procedures used to solve the equations are described and the general features of the solution are presented. The data of Ref. 1 were reanalyzed using these new fitting functions and the results are given in Sec. IV.

II. THE FADDEEV EQUATION

As discussed briefly in the Introduction, the Heitler equation or K-matrix equation used in Ref. 3 (hereafter called AW) was not a success. The functions generated, although suitably unitary, contained spurious first-sheet singularities. This difficulty is eliminated by using the full Faddeev equation. The solutions of this three-body Schrödinger equation are guaranteed to have correct analyticity properties.

We shall forego a full-scale derivation of the Faddeev equation from first principles, instead merely indicating how the K-matrix equation used in AW can be "promoted" to a corresponding Faddeev equation. The essential difference between a

Faddeev equation and the corresponding K-matrix equation is that the Schrödinger Green's function

$$\frac{1}{W-E-i\epsilon}=\mathrm{P}\,\frac{1}{W-E}+i\pi\delta(W-E) \tag{2.1}$$

in the Faddeev equation is replaced by its imaginary part $i\pi\delta(W-E)$ to obtain the K-matrix equation. We shall reverse this process, starting with the K-matrix equation [AW, Eq. (2.25)]

$$\mathcal{S}_a^{JPi}(s_1)=\delta_{ai}\mathcal{R}_i(s_1)+ie^{i\delta_a}\sin\delta_a\sum_b\int_{-1}^{1}d(\cos\chi_1)\,\mathcal{K}_{ab}(1,2)\times\mathcal{S}_b^{JPi}(s_2)\,. \tag{2.2}$$

This equation has already been simplified as much as possible. The notation is defined in the Appendix of AW and, in particular, we shall need the kinematic relations

$$s_2=\tfrac{1}{2}(W^2+3m_\pi^2-s_1)+2p_1q_1\frac{W}{\sqrt{s_1}}\cos\chi_1\,, \tag{2.3}$$

$$W=(p_2^2+s_2)^{1/2}+(p_2^2+m_\pi^2)^{1/2}=\omega_1+\omega_2+\omega_3\,, \tag{2.4}$$

$$\omega_3^2=m_\pi^2+p_1^2+p_2^2+2p_1p_2\cos\theta_{12}\,. \tag{2.5}$$

The replacement of the imaginary part of (2.1) by the full Green's function is not a uniquely defined process because the invariant mass of the two-body system (e.g., $\sqrt{s_2}$) and the momentum of the third particle (e.g., p_2) are now independent variables which together determine the value of W, rather than being related by the condition that W have the fixed value E. In particular we could have introduced a Green's function proportional to $2W/[W^2-(E+i\epsilon)^2]$ as was done in Ref. 17. However, we shall use the simpler choice and in Eq. (2.2) make the replacement

$$i=i\int dW\,\delta(W-E)\to\frac{1}{\pi}\int dW\,\frac{1}{W-E-i\epsilon}\,. \tag{2.6}$$

We must also replace the single variable s_1 in the function $\mathcal{S}_a^{JPi}(s_1)$ by the two variables s_1 and p_1 or, equivalently, by $q_1=(s_1/4-m_\pi^2)^{1/2}$ and p_1.

With these substitutions in Eq. (2.2) we find a double integral over W and $\cos\chi_1$. Changing variables with the aid of (2.3)–(2.5), we obtain in place of (2.2)

$$\mathcal{S}_a^{JPi}(p_1,q_1)=\delta_{ai}\mathcal{R}_i(p_1,q_1)+\left(\frac{8\pi\sqrt{s_1}}{q_1}\,e^{i\delta_a}\sin\delta_a\right)\frac{1}{8\pi^2}\sum_b\int_0^\infty\frac{p_2^2dp_2}{\omega_2}\int_{-1}^{1}\frac{d\cos\theta_{12}}{\omega_3(W-E-i\epsilon)}\mathcal{K}_{ab}(1,2)\mathcal{S}_b^{JPi}(p_2,q_2)\,. \tag{2.7}$$

The q_1 dependence is removed from $\mathcal{S}_a^{JPi}(p_1,q_1)$ by the ansatz

$$\mathcal{S}_a^{JPi}(p_1,q_1)=V_{S_a}(q_1)\tau_{S_a}(\sigma_1)W_a^{JPi}(p_1)\,, \tag{2.8}$$

which would be appropriate to a separable two-body interaction. Here σ_1 is a function of p_1 (see below) and all of the q_1 dependence is described by the functions

$$V_S(q)=\left(\frac{q}{q_R}\right)^S F_S(q^2)\,, \tag{2.9}$$

which contain a threshold factor and a form factor for the two-body resonance of spin S (the notation is adequate since there is only one resonance for each spin $S=0,1,2$). We used

$$F_S(q^2)=\left[1+\left(\frac{q}{1\ \mathrm{GeV}}\right)^4\right]^{-1}. \tag{2.10}$$

This is flat in the resonance region ($q_R\simeq 0.360$ GeV for the ρ) and provides a cutoff for $|q|\gg 1$ GeV for both real and pure imaginary q. The factor $\tau_S(\sigma)$ is the propagator for the two-body resonance. It is defined by the on-shell condition

$$V_S^2(q)\tau_S(\sigma)=\frac{8\pi\sqrt{\sigma}}{q}\,e^{i\delta_S}\sin\delta_S\,, \tag{2.11}$$

and σ is the on-shell s obtained by setting $W=E$ in (2.4) and solving for s:

$$\sigma=E^2-2E\omega+m_\pi^2\,. \tag{2.12}$$

In the on-shell Eq. (2.11) $q=(\sigma/4-m_\pi^2)^{1/2}$. We used the same Breit-Wigner resonance formulas as AW (see Table I of AW)

$$e^{i\delta_S}\sin\delta_S=\frac{M_R\Gamma}{M_R^2-\sigma-iM_R\Gamma}\,, \tag{2.13}$$

$$\Gamma=\left(\frac{q}{q_R}\right)^{2S+1}\frac{M_R}{\sqrt{\sigma}}\,\Gamma_R\,. \tag{2.14}$$

Substituting (2.9), (2.13), (2.14) into (2.11) we find

$$\tau_S(\sigma)=\frac{8\pi M_R^2\Gamma_R}{q_RF_S^2(q^2)}\,\frac{1}{M_R^2-\sigma-iM_R\Gamma}\,. \tag{2.15}$$

A substitution similar to (2.8) is made for the inhomogeneous term $\mathcal{R}_i$ of (2.7):

$$V_S(q_1)\tau_S(\sigma_1)X_i(p_1)=\mathcal{R}_i=\frac{q_1^Sp_1^L}{M_R^2-\sigma_1-iM_R\Gamma}\,, \tag{2.16}$$

i.e.,

$$X_i(p_1)=\frac{q_R^{S+1}F_S(q^2)}{8\pi M_R^2\Gamma_R}\,p_1^L\,. \tag{2.17}$$

In (2.17) q is a function of p_1 as specified in the next paragraph.

With the substitutions (2.8) and (2.16), the Faddeev equation (2.7) becomes

$$W_a^{JPi}(p_1)=\delta_{ai}X_i(p_1)+\frac{1}{8\pi^2}\sum_b\int_0^\infty\frac{p_2^2dp_2}{\omega_2}\int_{-1}^{1}\frac{d\cos\theta_{12}}{\omega_3(W-E-i\epsilon)}\mathcal{K}_{ab}(1,2)V_a(q_1)\tau_b(\sigma_2)V_b(q_2)W_b^{JPi}(p_2)\,. \tag{2.18}$$

In this equation $\tau_b(\sigma_2)$ is calculated from (2.15) using $\sigma_2=E^2-2E\omega_2+m_\pi^2$, $\omega_2=(p_2^2+m_\pi^2)^{1/2}$, and the q's in (2.15) are evaluated at $q=(\sigma_2/4-m_\pi^2)^{1/2}$. The inhomogeneous term $X_i(p_1)$ is calculated from (2.17) and the q's in that formula are given by $q=(\sigma_1/4-m_\pi^2)^{1/2}$, $\sigma_1=E^2-2E\omega_1+m_\pi^2$, $\omega_1=(p_1^2+m_\pi^2)^{1/2}$. On the other hand, the factors $V_a(q_1)$, $V_b(q_2)$ are functions of p_2 and $\cos\theta_{12}$ since they are calculated off the mass shell: $q_1=(s_1/4-m_\pi^2)^{1/2}$, $s_1=W^2-2W\omega_1+m_\pi^2$, $q_2=(s_2/4-m_\pi^2)^{1/2}$, $s_2=W^2-2W\omega_2+m_\pi^2$, with W and ω_3 given by (2.4), (2.5). All this constitutes, of course, an interpretation of how one should go off the mass shell. Using $\tau(\sigma_2)$ with σ_2 calculated from E appears to us consistent with the choice of an energy denominator $W-E-i\epsilon$ for the three-body problem during those periods when two particles are interacting to form a Breit-Wigner resonance and the third particle is a spectator.

There is a minor technical difficulty with the resonance form expressed by (2.13) and (2.14). Since the variable p_2 runs from 0 to $+\infty$, the function $\tau_S(\sigma_2)$ is needed for values of σ_2 from $-\infty$ to $\sigma_{max}=(E-m_\pi)^2$. Thus the form given in Eq. (2.15), which is reasonable for physical values of σ, needs to be modified to avoid several unpleasant features. The first of these is the singular factor $1/\sqrt{\sigma}$ in the function Γ. We chose to replace this by $1/2m_\pi$ for $\sigma<4m_\pi^2$. However, for large negative σ, the resulting function Γ grows as $(\sqrt{-\sigma})^{2S+1}$ so, for $S=1$, this overtakes the linear term $m_R^2-\sigma$ and has the sign to produce a pole in $\tau(\sigma)$ at $\sigma=-2.2$ GeV^2. To avoid this we also chose to change the sign of Γ for $\sigma<4m_\pi^2$ for $S=1$ only. Although this procedure could certainly be criticized as not analytic, the resulting function τ is small in this region, and we believe our results are insensitive to the details of τ in this region. An alternative analytic form using an effective-range formula similar to that of Chew and Mandelstam[19] could be used. In this modification the resonance denominator $m_R^2-\sigma-im_R\Gamma$ is replaced by

$$m_R^2-\sigma+\frac{m_R\Gamma_R}{\pi}\ln\frac{m_R-2q_R}{m_R+2q_R}-\frac{m_R\Gamma}{\pi}\ln\frac{2q-\sqrt{\sigma}}{2q+\sqrt{\sigma}}\,, \tag{2.19}$$

which has none of the above unpleasant features and is compared with our choice in Fig. 1. The differences appear to be minor. We did not use this form because it differs slightly in the physical region from the form used in the original fitting of Refs. 1 and 2.

III. SOLUTION OF THE FADDEEV EQUATION

In this section we discuss the method we used to solve the Faddeev equation (2.18). In order to avoid the singularities in this equation many authors have employed a method involving rotation of the p_2 integration contour into the complex plane.[20,21,17] We have used a more straightforward method, which stays with real variables p_1, p_2 and attacks the singularities directly. This turned out to be much less difficult and to take less computer time than we thought it would when we started. We want to describe this method in sufficient detail so that others might use it, since the method obviously has an applicability broader than the particular problem we solved with it.

The singularities in Eq. (2.18) arise from the pole $(W-E-i\epsilon)^{-1}$, which, after integration over $\cos\theta_{12}$ (at fixed p_1 and p_2), leads to logarithmic singularities at the edges of the Dalitz plot. Referring to (2.4), (2.5) we see that the physical re-

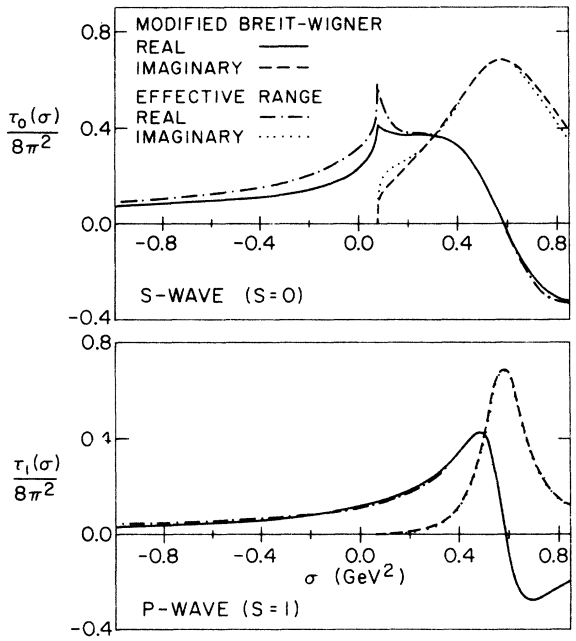

FIG. 1. Comparison of two forms for the two-pion propagator functions, $\tau_S(\sigma)$, as functions of the two-pion invariant-mass squared, σ. The real (imaginary) parts of the Breit-Wigner form which we used [Eq. (2.15) and (2.14) modified as described in the paragraph preceeding Eq. (2.19)] are shown by the solid curve (dashed curve). The real (imaginary) part of the effective-range form [Eq. (2.19)] is shown by the dash-dotted curve (dotted curve). The upper (lower) graphs correspond to spin zero (one) in the two-pion system.

gion (the interior of the Dalitz plot) is given by

$$W_{\min} \le E \le W_{\max}, \tag{3.1}$$

where

$$\begin{aligned} W_{\max} &= (p_1^2+m_\pi^2)^{1/2}+(p_2^2+m_\pi^2)^{1/2} \\ &\quad +[(p_1+p_2)^2+m_\pi^2]^{1/2}, \\ W_{\min} &= (p_1^2+m_\pi^2)^{1/2}+(p_2^2+m_\pi^2)^{1/2} \\ &\quad +[(p_1-p_2)^2+m_\pi^2]^{1/2}. \end{aligned} \tag{3.2}$$

Setting $W_{\max}=E$ or $W_{\min}=E$ to find the edges of the Dalitz plot, we obtain for the upper or lower boundaries p_{2Du}, p_{2Dl} at given p_1 the formulas

$$p_{2Du} = \tfrac{1}{2}p_1 + q_1(E-\omega_1)/\sqrt{\sigma_1}, \tag{3.3}$$

$$p_{2Dl} = \left|\tfrac{1}{2}p_1 - q_1(E-\omega_1)/\sqrt{\sigma_1}\right|, \tag{3.4}$$

where $\sigma_1 = E^2 - 2E\omega_1 + m_\pi^2$, $q_1 = (\sigma_1/4 - m_\pi^2)^{1/2}$, $\omega_1 = (p_1^2+m_\pi^2)^{1/2}$. For q_1 real, $\sigma_1 \ge 4m_\pi^2$. Thus the Dalitz plot lies inside the square region defined by

$$\omega_1 < \omega_D, \quad \omega_2 < \omega_D, \quad \omega_D = (E^2 - 3m_\pi^2)/2E. \tag{3.5}$$

It is convenient to explicitly separate off the singularities in the kernel of (2.18), leaving an integral of a smooth function to be done by Gaussian quadrature. To this end we add and substract a term in the numerator of the integration over $\cos\theta_{12}$. The Faddeev equation (2.18) can be written in the form

$$W_a^{JPi}(p_1) = \delta_{ai}X_i(p_1) + \sum_b \int_0^\infty dp_2\, K_{ab}(p_1,p_2) W_b^{JPi}(p_2), \tag{3.6}$$

where the kernel $K_{ab}(p_1,p_2)$ is given by

$$K_{ab}(p_1,p_2) = \frac{\tau_b(\sigma_2)}{8\pi^2}\frac{p_2^2}{\omega_2}\int_{-1}^{1}\frac{d\cos\theta_{12}}{\omega_3}\frac{\mathcal{K}_{ab}(1,2)V_a(q_1)V_b(q_2)}{W-E-i\epsilon}. \tag{3.7}$$

This kernel can be expressed as the sum of three terms:

$$K_{ab}(p_1,p_2) = iK_{ab}^{(1)}(p_1,p_2) + K_{ab}^{(2)}(p_1,p_2) + K_{ab}^{(3)}(p_1,p_2). \tag{3.8}$$

The term $K_{ab}^{(1)}(p_1,p_2)$ is the contribution from the δ-function term when we substitute (2.1) for the energy denominator in (3.7) and use $d\cos\theta_{12} = (\omega_3/p_1p_2)dW$ from (2.4), (2.5):

$$K_{ab}^{(1)}(p_1,p_2) = \begin{cases} \dfrac{\tau_b(\sigma_2)}{8\pi}\dfrac{p_2}{p_1\omega_2}V_a(\bar{q}_1)V_b(\bar{q}_2)K_{ab}(\bar{1},\bar{2}), & W_{\min} < E < W_{\max} \\ 0, \quad \text{otherwise}. \end{cases} \tag{3.9}$$

Here the barred variables in V_a, V_b, and $\mathcal{K}_{ab}$ indicate that $\cos\theta_{12}$ has the value $\cos\bar{\theta}_{12}$ such that $W=E$ and that other variables which depend on $\cos\theta_{12}$ are evaluated accordingly. If only the contribution $K_{ab}^{(1)}(p_1,p_2)$ is kept, the calculations in the present work reduce to those in AW, albeit done in a somewhat different way.

To eliminate the principal-value integral in the remainder of (3.7) we add and subtract a term, so as to cancel the pole:

$$K_{ab}^{(2)}(p_1,p_2) = \frac{\tau_b(\sigma_2)}{8\pi^2}\frac{p_2^2}{\omega_2}\int_{-1}^{1}\frac{d\cos\theta_{12}}{\omega_3}\,\mathrm{P}\frac{1}{W-E}\left[\mathcal{K}_{ab}(1,2)V_a(q_1)V_b(q_2) - \mathcal{K}_{ab}(\bar{1},\bar{2})V_a(\bar{q}_1)V_b(\bar{q}_2)\right], \tag{3.10}$$

$$K_{ab}^{(3)}(p_1,p_2) = \frac{\tau_b(\sigma_2)}{8\pi^2}\frac{p_2}{p_1\omega_2}\mathcal{K}_{ab}(\bar{1},\bar{2})V_a(\bar{q}_1)V_b(\bar{q}_2)\ln\left|\frac{W_{\max}-E}{W_{\min}-E}\right|. \tag{3.11}$$

For $W_{\min} \le E \le W_{\max}$ the subtraction point which defines the barred variables is $\bar{W}=E$, the same as used in (3.9). For $W_{\min} > E$ we use a subtraction point $\bar{W}=W_{\min}$ and for $W_{\max} < E$, $\bar{W}=W_{\max}$. With this choice $K_{ab}^{(2)}$ is a continuous function, and $K_{ab}^{(3)}$ contains the logarithmic singularities at $W_{\max}=E$ and $W_{\min}=E$. Study of the geometry yields the values given in Table I for the angles which enter the crossing matrix $\mathcal{K}_{ab}(\bar{1},\bar{2})$ for the cases $W_{\min}$

TABLE I. Angles in crossing matrix at subtraction points for Eqs. (3.9)–(3.11).

$W_{\min} > E$		$\cos\bar{\theta}_{12} = -1$
	$p_1 > 2p_2$	$\cos\bar{\chi}_1 = 1$, $\cos\bar{\chi}_2 = -1$
	$p_2 > 2p_1$	$\cos\bar{\chi}_1 = -1$, $\cos\bar{\chi}_2 = 1$
	$\frac{1}{2}p_2 < p_1 < 2p_2$	$\cos\bar{\chi}_1 = -1$, $\cos\bar{\chi}_2 = -1$
$W_{\max} < E$		$\cos\bar{\theta}_{12} = 1$
		$\cos\bar{\chi}_1 = 1$, $\cos\bar{\chi}_2 = 1$

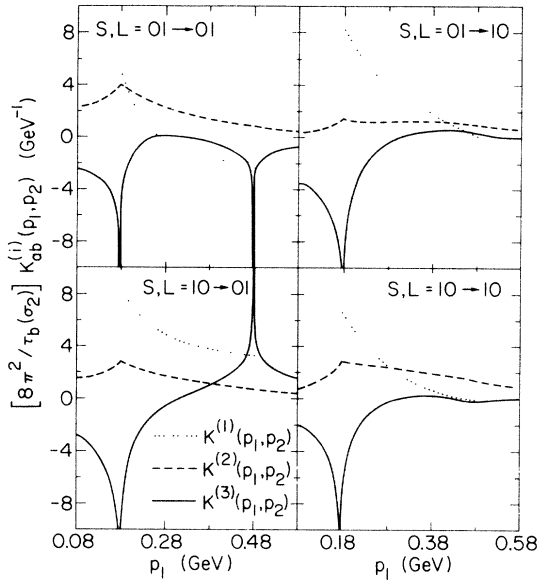

FIG. 2. The kernel of Eq. (3.6). The quantities plotted are $[8\pi^2/\tau_b(\sigma_2)]K_{ab}^{(i)}(p_1,p_2)$ as functions of p_1 at fixed $p_2=0.300$ GeV, $E=1.05$ GeV for the two coupled $J^P=1^+$ channels $1^+P(\epsilon\pi)$, $1^+S(\rho\pi)$. The dotted, dashed, and solid curves give, respectively, $K^{(1)}$, $K^{(2)}$, $K^{(3)}$ [see Eqs. (3.8)–(3.11)].

$>E$ and $W_{\max}<E$.

It is easy enough to evaluate $K_{ab}(p_1,p_2)$ numerically. For $K_{ab}^{(2)}(p_1,p_2)$ we used 12-point Gaussian quadrature. The logarithmic singularity in $K_{ab}^{(3)}(p_1,p_2)$ is explicit. We present in Fig. 2 plots of the three quantities $[8\pi^2/\tau_b(\sigma_2)]K_{ab}^{(i)}(p_1,p_2)$, $i=1,2,3$, as functions of p_1 at a fixed $p_2=0.300$ GeV, $E=1.05$ GeV for the two coupled $J^P=1^+$ channels $1^+P(\epsilon\pi)$, $1^+S(\rho\pi)$. The logarithmic singularities at the edges of the Dalitz plot are evident. For those states with the final $S_a=1$, threshold factors $q_1^{S_a}$ suppress the logarithmic singularities at the upper edge of the Dalitz plot for the particular p_2 chosen. Some impression can be formed from the graphs of the relative size of the three components. Recall that the K-matrix calculation of AW is duplicated by keeping only $K_{ab}^{(1)}$, which vanishes outside the Dalitz plot.

In order to eliminate the square-root singularities at the upper limits of the Dalitz plot at

$$p=p_D=(\omega_D^2-m_\pi^2)^{1/2}, \tag{3.12}$$

where ω_D is given by (3.5), we made a change of variable,

$$0\le p\le p_D,\quad -1\le x\le 0,\quad p=p_D\left\{1-\left[\frac{x(1-\alpha_1 x)}{1+\alpha_1}\right]^2\right\}, \tag{3.13}$$

$$p_D\le p\le\infty,\quad 0\le x\le 1,\quad p=p_D\left[1+\left(\frac{\alpha_2 x}{1-x}\right)^2\right]. \tag{3.14}$$

We chose $\alpha_1=0.2$, $\alpha_2=1.0$. The shape of the Dalitz plot in terms of these variables is shown in Fig. 3 for $E=1.14$ GeV.

The integral equation to be solved is thus of the form

$$f(x)=g(x)+\int_{-1}^{1}dx'K(x,x')f(x'), \tag{3.15}$$

where the kernel $K(x,x')$ has logarithmic singularities at the edges of a Dalitz plot such as indicated in Fig. 3. For a multichannel problem f and g are vectors and K is a matrix; we suppress this necessary but irrelevant complication for the moment. Although the kernel $K(x,x')$ has singularities, the solution $f(x)$ of the integral equation (3.15) is a smooth function except at $x=0$, where it is continuous. It is quite adequately represented by its values on an evenly spaced grid of points. In practice we used 25 evenly spaced points in the region $-1\le x\le 0$ and 12 evenly spaced points in the region $0\le x\le 1$. Some adjustments were made to avoid the special values $x=0$, ± 1. Since the kernel $K(x,x')$ contains singularities, the integral in (3.15) must be done carefully, especially near the singular points. Thus we use many more than 25 + 12 points to do the integral in (3.15), and to accomplish this we had to interpolate $f(x)$ between the points on which it is defined. Suppose the values of $f(x)$ on the 25 + 12 points x_i are f_i:

$$f_i=f(x_i). \tag{3.16}$$

Then with suitable interpolation functions $p_i(x)$ we take as approximation to $f(x)$

$$f(x)=\sum_i f_i p_i(x). \tag{3.17}$$

We used a standard interpolation scheme: For a given x find the three nearest x_i and use quadratic interpolation between the three corresponding values f_i. It is important to note that with this definition $p_i(x)$ is a rather curious discontinuous function:

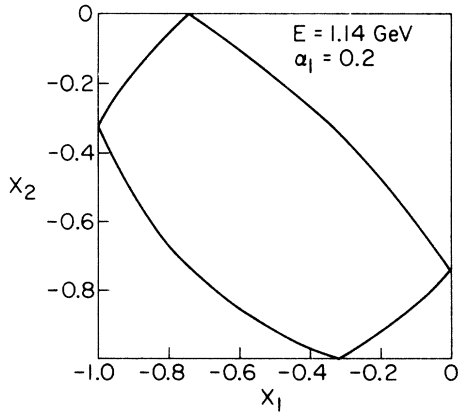

FIG. 3. The boundaries of the Dalitz plot in terms of the variables x_1, x_2 for $E=1.14$ GeV, $\alpha_1=0.2$ [see Eq. (3.13)].

$$p_i(x)=\begin{cases}0, & x<x_i-\frac{3}{2}\Delta\\ \frac{1}{2}\left(\frac{x-x_i}{\Delta}+2\right)\left(\frac{x-x_i}{\Delta}+1\right), & x_i-\frac{3}{2}\Delta<x<x_i-\frac{1}{2}\Delta\\ 1-\left(\frac{x-x_i}{\Delta}\right)^2, & x_i-\frac{1}{2}\Delta<x<x_i+\frac{1}{2}\Delta\\ \frac{1}{2}\left(\frac{x-x_i}{\Delta}-2\right)\left(\frac{x-x_i}{\Delta}-1\right), & x_i+\frac{1}{2}\Delta<x<x_i+\frac{3}{2}\Delta\\ 0, & x>x_i+\frac{3}{2}\Delta,\end{cases} \tag{3.17}$$

where $\Delta=x_i-x_{i-1}$ is the spacing for the x grid. There are further complications near the ends of the interval. If the program is properly constructed one can avoid thinking very much about these discontinuous functions, but it is important to note their existence for the subsequent integration.

Substituting (3.17) into (3.15) we find

$$f_i=g_i+\sum_j A_{ij}f_j, \tag{3.18}$$

where A_{ij} is given by

$$A_{ij}=\int_{-1}^{1} dx' K(x_i,x')p_j(x'). \tag{3.19}$$

For the x' integration we used a large number of Gaussian-quadrature points so as to get a good approximation to the integrals over the singular kernel $K(x,x')$. Now it is well known that Gaussian quadrature loses its tremendous power if one integrates across discontinuities. Therefore, to avoid the discontinuities in $p_j(x')$ in the integral (3.19) we used Gaussian quadrature on intervals with end points midway between the x_i, namely $x_i-\Delta/2$ to $x_i+\Delta/2$. For each such interval we used 12-point Gaussian quadrature.

For the special intervals which straddled the edges of the Dalitz plot and which contain the logarithmic singularities in $K(x,x')$ we put in more points. For each x_i in (3.19) the program locates the x_j such that an edge x_D of the Dalitz plot lies between $x_j-\Delta/2$ and $x_j+\Delta/2$. We then used 24-point (ordinary, *not* logarithmic) Gaussian quadrature for the interval $x_j-\Delta/2$ to x_D and a separate 24-point Gaussian quadrature for the interval x_D to $x_j+\Delta/2$. In this way the 37×37 matrix A_{ij} of (3.19) is calculated with $(25+13-2)\times12+4\times24=528$ points for the x' integration.

The rest of the solution of the integral equation (3.15) involves just the standard inversion of the matrix $(\delta_{ij}-A_{ij})$ which appears in (3.18). The numbers of integration points mentioned in the description above seemed adequate to give good numerical accuracy. Doubling the number of integration points produced no significant changes in the answers.

In order to carry out the fitting procedure described in Sec. IV we have solved the equations described above for the coupled channels $J^PL(S)=0^-S(\epsilon\pi)$ and $0^-P(\rho\pi)$ and also for the coupled channels $1^+P(\epsilon\pi)$ and $1^+S(\rho\pi)$ at energies $E=0.86$ GeV to 1.50 GeV in steps of 0.04 GeV. This required some 23 hours of computer time on a PDP-10 with a KA10 processor, which has a computing speed approximately $\frac{1}{10}$ that of a CDC 6600.

In Figs. 4 and 5 we present some results from the computer calculation at one energy $E=1.18$ GeV, for the coupled channels $1^+P(\epsilon\pi)$, $1^+S(\rho\pi)$. Figure 4 gives real parts, Fig. 5 imaginary parts. The four graphs in each figure give the coupling of each channel to itself and to its partner. Three calculations are compared on the graphs: the solid curves are the results from the calculation

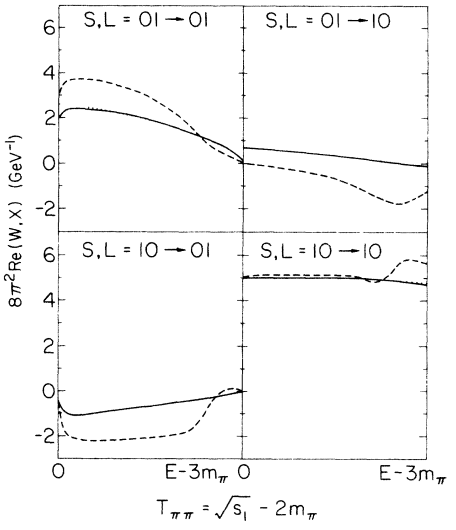

FIG. 4. The real parts of $8\pi^2 W_a^{JPi}$ and $8\pi^2 X_i$ as functions of the dipion kinetic energy $T_{\pi\pi}=\sqrt{s_1}-2m_\pi$ at $E=1.18$ GeV for the two coupled $J^P=1^+$ channels $1^+P(\epsilon\pi)$, $1^+S(\rho\pi)$. The solid curves give the solutions $8\pi^2 W_a^{JPi}$ of Eq. (3.6); the dotted curves give the inhomogeneous terms $8\pi^2 X_i$. The dashed curves give the solutions $8\pi^2 W_a^{JPi}$ when the contributions $K^{(2)}$ and $K^{(3)}$ in (3.8) are dropped; this is equivalent to the K-matrix calculation of Ref. 3.

described in this paper, the dotted curves are the inhomogeneous terms X_i [see Eq. (3.6)] (these real functions vanish for the off-diagonal elements), the dashed curves give the results from the K-matrix calculations of AW, equivalent to dropping $K^{(2)}$ and $K^{(3)}$ in (3.8). The curves are plotted vs the variable $\sqrt{s_1}=(E^2-2E\omega_1+m_\pi^2)^{1/2}$, and only the physical region, $m_\pi<\omega_1<\omega_D$ [see Eq. (3.5)] is shown. This is the part actually used in the fitting to be described in Sec. IV. In the unphysical region $p>p_D$ the solutions fall off with increasing p in a way which depends somewhat on the cutoff procedure [see Eq. (2.10)].

The most noteworthy feature of Figs. 4 and 5 is that the full Faddeev calculation described in this paper yields answers much closer to the inhomogeneous term than does the K-matrix calculation of AW. This is particularly so in the resonance region $\sqrt{s_1}\sim 0.78$ GeV, and we note that this portion of our solutions will be strongly enhanced when they are multiplied by the Breit-Wigner forms describing the ρ and ϵ resonances [see Eq. (2.8) and Fig. 1].

Thus it appears that the K-matrix calculation of AW produces spurious large effects, as explained by several authors,[9,10] and that in the solution of the full Faddeev equations the rescattering corrections are much smaller. To the extent that these rescattering effects are small we may expect a fitting analysis based on our functions W_a^{JPi} to

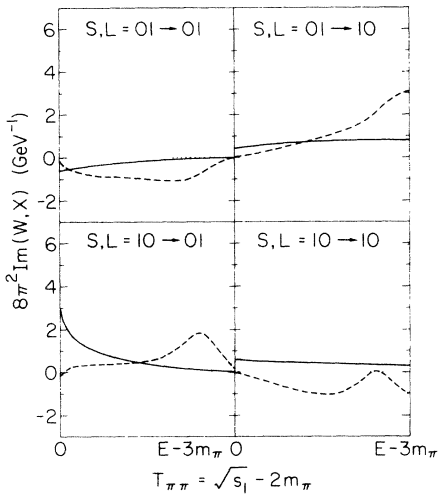

FIG. 5. The imaginary parts of $8\pi^2 W_a^{JPi}$ and $8\pi^2 X_i$ as functions of the dipion kinetic energy $T_{\pi\pi}=\sqrt{s_1}-2m_\pi$ at $E=1.18$ GeV for the two coupled $J^P=1^+$ channels $1^+P(\epsilon\pi)$, $1^+S(\rho\pi)$. The solid curves give the solutions $8\pi^2 W_a^{JPi}$ of Eq. (3.6); the dotted curves give the inhomogeneous terms $8\pi^2 X_i$. The dashed curves give the solutions $8\pi^2 W_a^{JPi}$ when the contributions $K^{(2)}$ and $K^{(3)}$ in (3.8) are dropped; this is equivalent to the K-matrix calculation of Ref. 3.

yield results similar to those obtained by using just the inhomogeneous terms X_i, as effectively done in the original analyses using the Ascoli program.[1,2] The graphs in Figs. 4 and 5 indicate that the effects we have calculated are not completely negligible, so their influence on the fits has to be checked.

As a final point, before going on to a discussion of these fits, we consider the possibility that the forces incorporated in our Faddeev equation are strong enough to generate or strongly modify three-pion resonances. We considered two facets of this question. First, in the course of solving Eq. (3.18) we evaluated the determinant of the matrix $(\delta_{ij}-A_{ij})$. For the $J^P=1^+$ state this has a small imaginary part ≤ 0.06 and the real part varies smoothly in the range 0.94 to 1.00 as E varies from 0.86 GeV to 1.50 GeV. There is no hint of resonant behavior in the 1^+ state. (One would expect the determinant to vanish at a resonance position in the complex plane and to vary rapidly as one moves along the real axis past the resonance pole.)

On the other hand, suppose an A_1 resonance is produced by some mechanism other than the pion-exchange forces considered in this paper, e.g., colored-gluon exchange between quarks. The pion-exchange processes considered here would still occur and might conceivably strongly change the character of the resonance, e.g., suppress the phase variation associated with a Breit-Wigner formula. We could suppose, for example, that gluon-exchange forces lead to a "bare" resonance described by a Breit-Wigner formula

$$\frac{1}{E_R-E-i\Gamma}. \tag{3.20}$$

Then self-energy bubbles of the sort indicated in Fig. 6 would lead to a self-energy correction which would change (3.20) to

$$\frac{1}{E_R-E-i\Gamma-\Sigma(E)}. \tag{3.21}$$

For a coupled-channel problem $\Sigma(E)$ has the form

$$\Sigma(E)=\gamma_a\gamma_b\Sigma_{ab}(E), \tag{3.22}$$

where the γ_a are couplings of the bare A_1 to the two channels $1^+S(\rho\pi)$, $1^+P(\epsilon\pi)$, and $\Sigma_{ab}(E)$ is a matrix given as an integral over the solution $W_a^{JPi}(p_1)$ of the integral equation (2.18):

$$\Sigma_{ab}(E)=\int_0^\infty \frac{p_1^2 dp_1}{\omega_1} X_a(p_1)\tau_{S_a}(\sigma_1)W_a^{JPb}(p_1)C(p_1). \tag{3.23}$$

Here $C(p_1)$ is a cutoff function, which we chose quite arbitrarily to have the form

$$C(p)=[1+(p/4p_D)^6]^{-1}. \tag{3.24}$$

In any event, while the cutoff provided by the form factor (2.10) leads to convergent integrals in the integral equation (2.18), an additional cutoff is needed to achieve a convergent self-energy integral (3.23). Unfortunately, with the cutoff procedure above, Σ_{ab} is not quite symmetric in a,b since the extra cutoff (3.24) is applied in the final state a but not the initial state b. Since the discussion of (3.21)–(3.23) is only a minor part of the present paper we thought it best not to include the extra cutoff (3.24) in the initial state for the whole calculation. We did some checking with such a cutoff included in the initial state and there seemed to be no change in qualitative conclusions.

We present some plots of $\Sigma_{ab}(E)$ as functions of E in Fig. 7. It would appear that these quantities are smooth slowly varying functions of E. To the extent that $\Sigma(E)$ can be approximated by a linear function $\Sigma(E) \simeq \Sigma(E_R) + \Sigma'(E_R)(E - E_R)$ the formula (3.21) can be written as a "pure" Breit-Wigner formula (3.20) with shifted position and width. We therefore believe that self-energy effects of the sort we have been discussing are incapable of distorting a bare Breit-Wigner resonance into some strange thing, which, for example, has no phase variation.

We hasten to add that whatever the form of an A_1 resonance, assuming it exists, whether pure as in (3.20) or of a more complicated type as in (3.21), the Ascoli fitting program should find it. Changing the functions used in this fitting program to our functions $W_a^{JPi}(p)$ is at best a more accurate description of the final breakup of the resonance into three pions, more accurate because the functions have better unitarity and analyticity properties.

IV. FITS TO DATA

Numerous workers have fitted data on three-pion production in the reaction $\pi^- p \to \pi^-\pi^+\pi^- p$ using Ascoli's program FIT.[1,2] Such fits always yield a big bump in the $1^+S(\rho\pi)$ partial wave with a peak near 1.20 GeV, but the phase of this wave relative to several other waves does not appear to exhibit the phase change characteristic of a resonance described by a Breit-Wigner formula.

The Ascoli program fits data to certain functions which can be supplied by the user. In the original work[1,2] these functions were the inhomogeneous terms in the integral equations (2.2) or (2.18) and

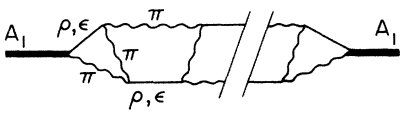

FIG. 6. Self-energy corrections which contribute to Eq. (3.21).

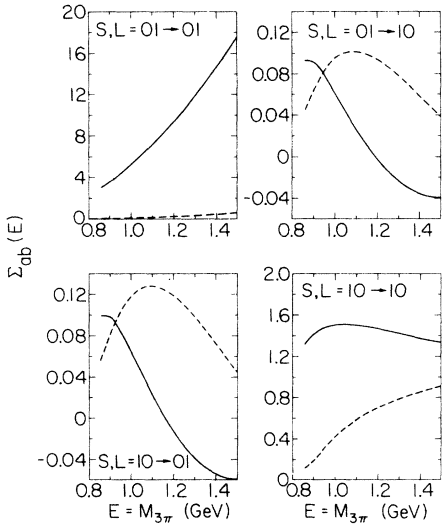

FIG. 7. The self-energy terms Σ_{ab} of Eq. (3.23) as functions of E for the two coupled $J^P = 1^+$ channels $1^+P(\epsilon\pi)$, $1^+S(\rho\pi)$. Solid curves give real parts, dashed curves imaginary parts.

the results were as described in the previous paragraph. This work was criticized on the grounds that the functions did not satisfy Watson's theorem. In AW (Ref. 3) this criticism was answered by using a K-matrix formalism; this

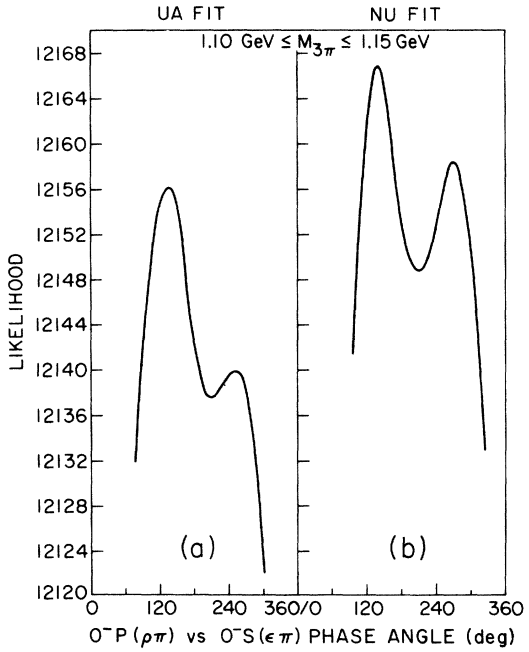

FIG. 8. Likelihood as a function of the $0^-P(\rho\pi)$ vs $0^-S(\epsilon\pi)$ relative phase angle for the bin 1.10 GeV$< M_{3\pi} <$ 1.15 GeV, other parameters being chosen so as to maximize the likelihood. Comparison of (a) the unitarized, analytic fits of the present work with (b) the nonunitary fits of Ref. 3.

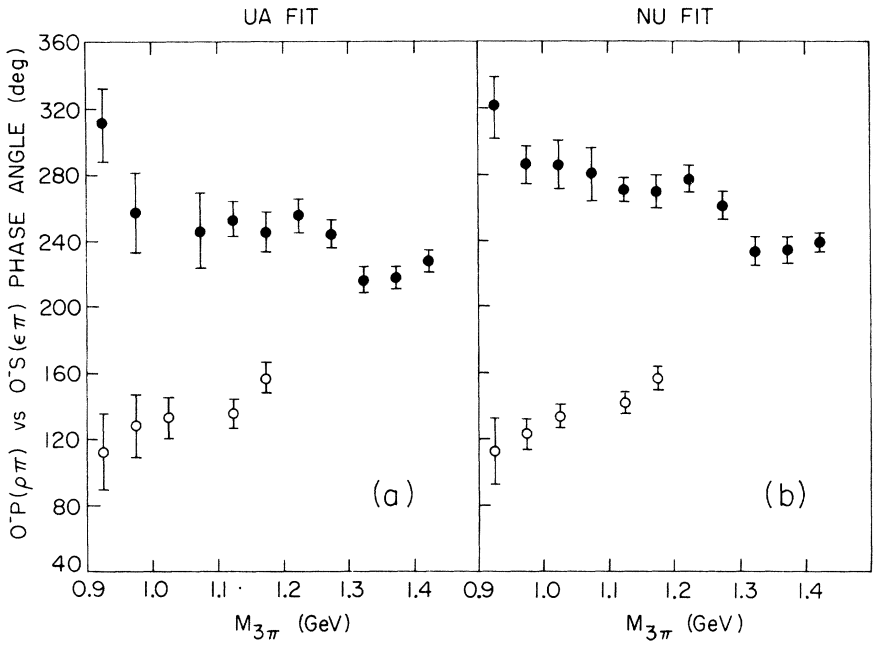

FIG. 9. The $0^-P(\rho\pi)$ vs $0^-S(\epsilon\pi)$ relative phase angle obtained in fits to the Serpukhov data (Refs. 1 and 2). The solid points correspond to the rightmost peaks in Figs. 8(a) and 8(b), the hollow points to the leftmost peaks in Figs. 8(a) and 8(b). Comparison of (a) the unitarized, analytic fits of the present work with (b) the nonunitary fits of Ref. 3.

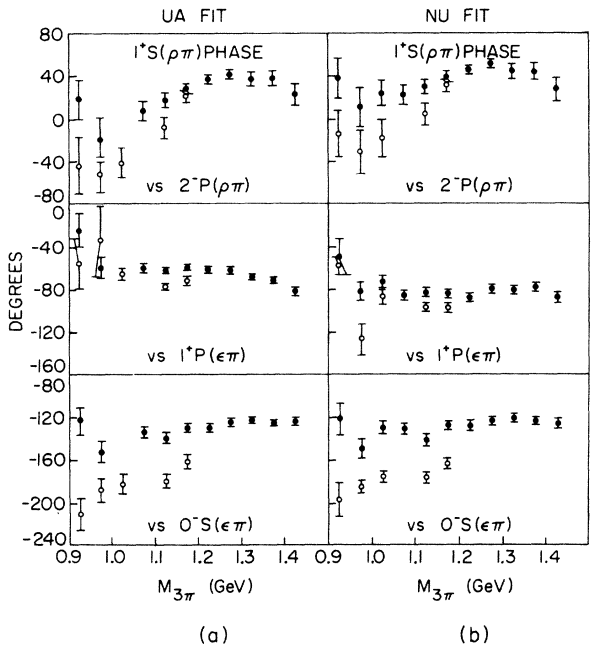

FIG. 10. The $1^+S(\rho\pi)$ phase relative to $2^-P(\rho\pi)$, $1^+P(\epsilon\pi)$, and $0^-S(\epsilon\pi)$ obtained in fits to the Serpukhov data (Refs. 1 and 2). The solid points correspond to the rightmost peaks in Figs. 8(a) and 8(b), the hollow points to the leftmost peaks in Figs. 8(a) and 8(b). Comparison of (a) the unitarized, analytic fits of the present work with (b) the nonunitary fits of Ref. 3.

amounts to keeping only the term $i\mathbf{K}^{(1)}(p_1,p_2)$ on the right-hand side of (3.8). This seemed to be a step backward in some respects since the fits were now significantly worse, as measured by χ^2. However, the conclusion about the lack of phase variation for the A_1 state seemed to remain.

Recently the lack of success of the K-matrix formalism has been criticized and explained as due to the generation of spurious first-sheet singularities.[9,10] In order to answer this second level of criticism, we have solved the full Faddeev equations, as described in Secs. II and III. In this section we discuss our results when we used these new, properly unitary and analytic, functions in Ascoli's program FIT.

In AW a large number of coupled states was kept in the calculation (see Table II of AW). In the present work we solved the coupled Faddeev equations for the $0^-S(\epsilon\pi), 0^-P(\rho\pi)$ states and the coupled equations for the $1^+P(\epsilon\pi)$ and $1^+S(\rho\pi)$ states. For the $2^-P(\rho\pi)$ and $2^+D(\rho\pi)$ states we used just the inhomogeneous terms of the integral equations. Thus the initial states are the same as in AW, but we drop all effects due to the f meson, neglect rescattering effects for 2^- and 2^+ states, and neglect the coupling to the $1^+D(\rho\pi)$ state. Some auxiliary checking indicated that the inclusion of this latter coupling in the integral equations had a negligible effect on the $1^+S(\rho\pi), 1^+P(\epsilon\pi)$ coupled states and that rescattering makes little change in the 2^- and 2^+ states. We made the same assumptions

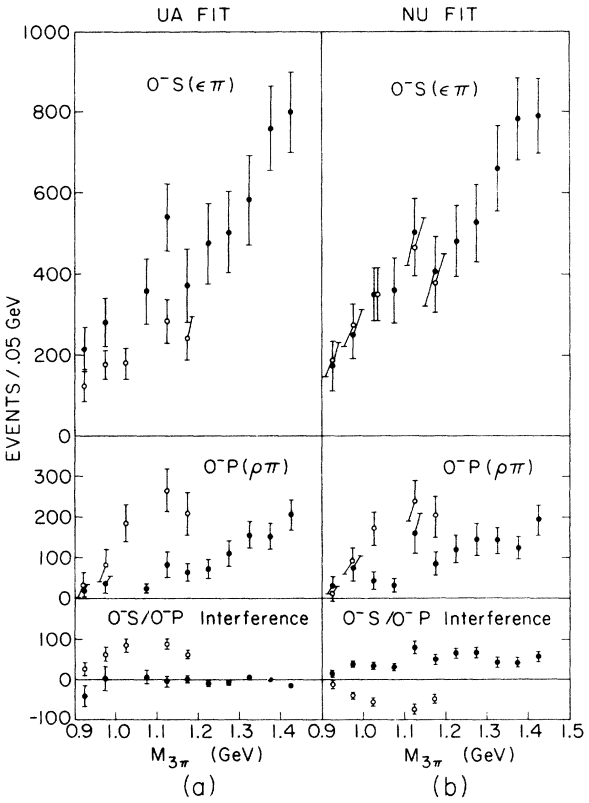

FIG. 11. The number of events per 0.05 GeV for the 0^- states as obtained in fits to the Serpukhov data (Refs. 1 and 2). The notation is the same as in Figs. 9 and 10.

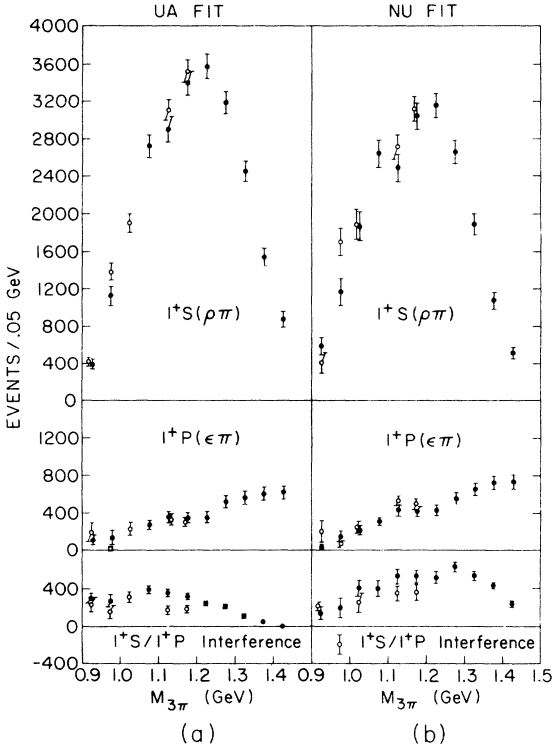

FIG. 12. The number of events per 0.05 GeV for the 1^+ states as obtained in fits to the Serpukhov data (Refs. 1 and 2). The notation is the same as in Figs. 9 and 10.

about isospin as AW. Finally, the CERN-IHEP data[1,2] fit was the same as used in AW.

The fits with the new functions are much better than those obtained in AW. They are still not quite as good as the original fits obtained with just the inhomogeneous terms of the integral equations.[2] The χ^2 differences between the present unitary, analytic fits and the original nonunitarized fits are $\lesssim 40$ as compared to differences ranging up to almost 500 for the unitarized vs nonunitarized fits (see Fig. 7 of AW). These differences of ~40 could presumably be reduced further by keeping more states in the coupled equations. We feel that the unphysical features of the unitarized functions have been eliminated in the new solutions of the Faddeev equations. However, it does seem noteworthy that despite all the effort to date we have not succeeded in doing better than was obtained with the simple isobar functions which form the inhomogeneous terms of our integral equations. The moral for future fitters would seem to be that it is not worth the effort to try to do better than the isobar model.

Since the main issue of physical interest would seem to be the phase change or lack thereof for the A_1 state, we shall confine the discussion of our new fits to that point.

The first thing one finds when making a large number of fits is that there is an ambiguity in the $0^-P(\rho\pi)$ vs $0^-S(\epsilon\pi)$ phase angle, i.e., the likelihood obtained by the fitting program is a double-humped function of this angle, the two peaks differing in likelihood by $\lesssim 10$ units. An example of this is provided in Fig. 8, where we show plots of the likelihood vs this phase angle for the bin $1.10\ \text{GeV} < M_{3\pi} < 1.15\ \text{GeV}$. In this figure and those that follow the results obtained with the new unitary, analytic (UA) solutions of the Faddeev equation are compared with results obtained with the nonunitary (NU) inhomogeneous terms in the integral equations (the isobar model). In Fig. 9 we show plots of the two solutions for this phase angle as a function of 3π mass. For some 3π-mass bins there is a double-humped distribution and hence two solutions; for some bins there is a single-humped distribution and hence only one solution. At the higher 3π masses the solution seems to be unique. In most former reports on fits a principle of continuity has been invoked to pick out the upper branch in Fig. 9(b), i.e., other quantities, e.g., other phase angles, quoted are those corresponding to the local maximum associated with the upper branch of Fig. 9(b). For the bins (0.95–1.00) GeV, (1.00–1.05)

TABLE II. The results of the unitary, analytic (UA) fits compared to the nonunitary (NU) fits. Some of this information was presented in Figs. 9–12. The incomplete columns to the left in the table correspond to the lower branches (with hollow points) in Fig. 9, i.e., the leftmost peaks in Fig. 8. The data fitted was from the 25- and 40-GeV/c joint CERN-IHEP Serpukhov experiment (Refs. 1, 2).

Bin $M_{3\pi}$(GeV)	UA		NU		UA		NU	
		$0^-S(\epsilon\pi)$ events				$0^-P(\rho\pi)$ events		
0.90–0.95	123 ± 37	216 ± 54	187 ± 44	172 ± 64	33 ± 31	19 ± 16	12 ± 20	31 ± 21
0.95–1.00	175 ± 36	281 ± 59	272 ± 49	251 ± 62	82 ± 38	35 ± 22	91 ± 32	73 ± 31
1.00–1.05	177 ± 39		350 ± 61	351 ± 65	185 ± 45		172 ± 42	45 ± 20
1.05–1.10		357 ± 81		360 ± 78		26 ± 11		34 ± 16
1.10–1.15	285 ± 53	542 ± 85	465 ± 72	504 ± 82	266 ± 52	83 ± 31	240 ± 49	162 ± 51
1.15–1.20	242 ± 54	372 ± 91	379 ± 72	407 ± 85	208 ± 52	63 ± 22	204 ± 51	84 ± 28
1.20–1.25		476 ± 97		481 ± 87		72 ± 24		121 ± 37
1.25–1.30		504 ± 99		528 ± 95		110 ± 31		146 ± 40
1.30–1.35		581 ± 110		660 ± 105		156 ± 33		142 ± 31
1.35–1.40		758 ± 106		783 ± 103		152 ± 32		124 ± 28
1.40–1.45		796 ± 100		790 ± 92		205 ± 37		195 ± 37
		$0^-S/0^-P$ interference events				0^-P vs 0^-S phase (deg)		
0.90–0.95	27 ± 17	−42 ± 26	−12 ± 11	14 ± 7	112 ± 23	311 ± 23	112 ± 20	321 ± 20
0.95–1.00	63 ± 17	4 ± 28	−40 ± 8	38 ± 8	128 ± 19	258 ± 24	122 ± 9	285 ± 11
1.00–1.05	84 ± 17		−56 ± 10	35 ± 8	133 ± 12		133 ± 7	285 ± 14
1.05–1.10		6 ± 17		31 ± 9		246 ± 23		279 ± 16
1.10–1.15	87 ± 13	−5 ± 14	−73 ± 12	79 ± 15	135 ± 9	254 ± 10	141 ± 6	270 ± 7
1.15–1.20	62 ± 11	0 ± 9	−48 ± 12	50 ± 12	157 ± 9	245 ± 12	156 ± 7	269 ± 10
1.20–1.25		−11 ± 8		66 ± 13		255 ± 10		277 ± 8
1.25–1.30		−7 ± 6		68 ± 13		244 ± 8		261 ± 8
1.30–1.35		6 ± 5		43 ± 13		216 ± 8		233 ± 8
1.35–1.40		−1 ± 4		43 ± 12		217 ± 7		234 ± 8
1.40–1.45		−15 ± 4		58 ± 12		227 ± 6		238 ± 6
		$1^+S(\rho\pi)$ events				$1^+P(\epsilon\pi)$ events		
0.90–0.95	422 ± 52	393 ± 57	407 ± 111	590 ± 93	174 ± 107	119 ± 45	210 ± 117	44 ± 31
0.95–1.00	1379 ± 94	1123 ± 99	1699 ± 145	1163 ± 146	14 ± 18	143 ± 74	79 ± 21	158 ± 57
1.00–1.05	1907 ± 100		1881 ± 155	1869 ± 149	230 ± 76		250 ± 59	220 ± 50
1.05–1.10		2724 ± 123		2643 ± 146		272 ± 55		309 ± 45
1.10–1.15	3105 ± 111	2880 ± 137	2713 ± 135	2495 ± 146	330 ± 59	364 ± 58	531 ± 54	432 ± 57
1.15–1.20	3525 ± 114	3396 ± 129	3108 ± 135	3039 ± 136	290 ± 52	348 ± 55	491 ± 50	420 ± 55
1.20–1.25		3579 ± 130		3151 ± 133		353 ± 54		434 ± 56
1.25–1.30		3184 ± 124		2658 ± 124		523 ± 65		563 ± 63
1.30–1.35		2450 ± 113		1889 ± 107		562 ± 73		657 ± 70
1.35–1.40		1546 ± 94		1076 ± 86		613 ± 73		731 ± 71
1.40–1.45		879 ± 80		507 ± 64		616 ± 72		753 ± 70
		$1^+S/1^+P$ interference events				1^+S vs 1^+P phase (deg)		
0.90–0.95	233 ± 80	301 ± 43	211 ± 42	147 ± 69	−56 ± 24	−24 ± 16	−59 ± 8	−50 ± 17
0.95–1.00	153 ± 70	278 ± 57	−237 ± 123	157 ± 95	−33 ± 35	−59 ± 10	−128 ± 15	−83 ± 9
1.00–1.05	309 ± 54		259 ± 103	407 ± 82	−66 ± 5		−88 ± 7	−74 ± 6
1.05–1.10		391 ± 49		405 ± 83		−60 ± 4		−87 ± 5
1.10–1.15	169 ± 47	352 ± 40	356 ± 87	536 ± 77	−78 ± 3	−62 ± 3	−98 ± 4	−84 ± 4
1.15–1.20	185 ± 41	315 ± 32	361 ± 85	542 ± 71	−72 ± 4	−60 ± 3	−99 ± 4	−86 ± 4
1.20–1.25		244 ± 26		517 ± 68		−62 ± 3		−89 ± 4
1.25–1.30		210 ± 19		629 ± 59		−62 ± 3		−81 ± 4
1.30–1.35		110 ± 14		537 ± 51		−69 ± 3		−82 ± 4
1.35–1.40		55 ± 9		431 ± 39		−72 ± 3		−80 ± 4
1.40–1.45		15 ± 5		239 ± 34		−82 ± 4		−89 ± 5

TABLE II. (*Continued*)

Bin $M_{3\pi}$(GeV)	UA		NU		UA		NU	
	1^+S vs 0^-S phase (deg)				1^+S vs 2^-P phase (deg)			
0.90–0.95	−211 ± 14	−123 ± 13	−198 ± 16	−122 ± 15	−44 ± 27	18 ± 19	−15 ± 22	37 ± 19
0.95–1.00	−188 ± 11	−152 ± 10	−186 ± 6	−150 ± 9	−53 ± 17	−20 ± 21	−32 ± 21	10 ± 19
1.00–1.05	−183 ± 9		−176 ± 5	−130 ± 6	−42 ± 14		−19 ± 17	23 ± 12
1.05–1.10		−134 ± 5		−131 ± 5		7 ± 9		21 ± 9
1.10–1.15	−181 ± 7	−140 ± 5	−177 ± 5	−142 ± 6	−9 ± 10	16 ± 7	3 ± 10	29 ± 7
1.15–1.20	−162 ± 7	−130 ± 4	−164 ± 5	−128 ± 4	21 ± 6	27 ± 5	30 ± 6	38 ± 5
1.20–1.25		−130 ± 4		−128 ± 4		36 ± 4		45 ± 4
1.25–1.30		−125 ± 4		−124 ± 4		41 ± 4		50 ± 4
1.30–1.35		−123 ± 3		−121 ± 4		36 ± 6		43 ± 7
1.35–1.40		−126 ± 3		−124 ± 4		37 ± 7		43 ± 8
1.40–1.45		−124 ± 4		−126 ± 5		22 ± 10		26 ± 11
	2^+D vs 1^+S phase (deg)				2^+D vs 1^+P phase (deg)			
0.90–0.95	65 ± 67	−3 ± 62	33 ± 57	−28 ± 57	9 ± 65	−27 ± 62	−27 ± 56	−78 ± 57
0.95–1.00	70 ± 42	21 ± 71	56 ± 44	4 ± 75	37 ± 50	−38 ± 70	−72 ± 47	−79 ± 76
1.00–1.05	30 ± 50		19 ± 57	−41 ± 18	−36 ± 49		−69 ± 58	−115 ± 19
1.05–1.10		−2 ± 18		−14 ± 18		−62 ± 18		−101 ± 19
1.10–1.15	−31 ± 6	−34 ± 5	−42 ± 6	−45 ± 5	−109 ± 7	−96 ± 6	−140 ± 7	−129 ± 7
1.15–1.20	−31 ± 5	−32 ± 5	−39 ± 5	−41 ± 5	−104 ± 6	−93 ± 5	−138 ± 6	−127 ± 6
1.20–1.25		−31 ± 3		−39 ± 3		−93 ± 4		−128 ± 5
1.25–1.30		−14 ± 2		−22 ± 3		−76 ± 3		−102 ± 4
1.30–1.35		23 ± 3		16 ± 3		−46 ± 3		−66 ± 4
1.35–1.40		46 ± 4		37 ± 4		−27 ± 5		−42 ± 5
1.40–1.45		60 ± 7		54 ± 7		−22 ± 4		−35 ± 7
	$2^-P(\rho\pi)$ events				$2^+D(\rho\pi)$ events			
0.90–0.95	114 ± 39	123 ± 42	114 ± 38	132 ± 43	33 ± 18	33 ± 18	30 ± 18	33 ± 19
0.95–1.00	144 ± 47	145 ± 50	145 ± 49	169 ± 51	16 ± 17	18 ± 16	16 ± 18	20 ± 17
1.00–1.05	208 ± 52		242 ± 55	175 ± 61	33 ± 26		35 ± 27	31 ± 28
1.05–1.10		216 ± 67		218 ± 68		157 ± 32		145 ± 32
1.10–1.15	488 ± 79	501 ± 81	490 ± 80	509 ± 83	208 ± 41	219 ± 39	213 ± 41	215 ± 41
1.15–1.20	745 ± 84	747 ± 84	755 ± 83	711 ± 84	303 ± 40	306 ± 40	306 ± 40	291 ± 41
1.20–1.25		635 ± 87		591 ± 90		606 ± 53		590 ± 53
1.25–1.30		805 ± 89		757 ± 90		1491 ± 68		1468 ± 69
1.30–1.35		824 ± 88		777 ± 89		2064 ± 72		2048 ± 73
1.35–1.40		650 ± 78		605 ± 79		1019 ± 57		1002 ± 57
1.40–1.45		672 ± 71		637 ± 72		521 ± 46		515 ± 47

GeV, and (1.10–1.15) GeV the likelihood of the other solution is higher by $\lesssim$10 units, but this was thought to be overridden by the continuity argument.

For the new UA fits the situation seems more complicated. In addition to the lower branch in Fig. 9(a) having a higher likelihood for the (0.95–1.00)-GeV and (1.10–1.15)-GeV bins (by 16 units for the latter bin), there is a single-humped distribution leading to only one solution corresponding to the lower branch for the (1.00–1.05)-GeV bin. Thus the continuity argument is less compelling for the UA fits, and so we give phase angles corresponding to both branches in subsequent plots.

In Fig. 10 we present the relative phases of $1^+S(\rho\pi)$ vs $2^-P(\rho\pi)$, vs $1^+P(\epsilon\pi)$, and vs $0^-S(\epsilon\pi)$. In Figs. 11 and 12 are shown the amounts of production in each 0^- and 1^+ state. The numerical values of the fit parameters are given in Table II. The question now is what is the evidence for or against a phase variation in the A_1 state. The answer is not unambiguous. If one erases from the plot all hollow points, corresponding to lower-branch solutions in Fig. 9, the UA fits yield the same answer as obtained previously with NU fits: there is no evidence for the sort of rapid phase variation that one expects from a resonant state. If one draws curves connecting the hollow points (lower branch of Fig. 9) for the three lowest energy bins to the solid points (upper branch of Fig. 9) for the higher-energy bins, one obtains what could be interpreted as resonant behavior in the 1^+ state.

This seems to us highly suspect since the same exercise applied to Fig. 9 would appear to yield a resonance in the 0^-S wave. The safest procedure is of course to extend the error bars so that they cover both solutions and the interval between for those bins where there are two solutions. This leads to error bars so large one cannot really tell what is happening in the low-energy region.

The only safe conclusion would appear to be that with the present analysis of the present data there is no compelling evidence *for* a rapidly varying phase in the A_1 state. On the other hand, the present data does not completely rule out such a possibility.

ACKNOWLEDGMENT

We are greatly indebted to G. Ascoli and R. M. Brown for their assistance, without which this paper could not have been written.

---

*Work supported in part by the NSF under Grant No. PHY75-21590.

[1]Yu. M. Antipov *et al.*, Nucl. Phys. B63, 141 (1973).
[2]Yu. M. Antipov *et al.*, Nucl. Phys. B63, 153 (1973).
[3]G. Ascoli and H. W. Wyld, Phys. Rev. D 12, 43 (1975).
[4]G. Ascoli *et al.*, Phys. Rev. D 9, 1963 (1974).
[5]R. F. Peierls, Phys. Rev. Lett. 6, 641 (1961).
[6]M. Nauenberg and A. Pais, Phys. Rev. Lett. 8, 82 (1962).
[7]C. Goebel, Phys. Rev. Lett. 13, 143 (1964).
[8]G. Fox, in *Experimental Meson Spectroscopy—1972*, proceedings of the Third International Conference, Philadelphia, edited by K. W. Lai and A. H. Rosenfeld (AIP, New York, 1972), p. 271.
[9]I. J. R. Aitchison and R. J. A. Golding, Phys. Lett. 59B, 288 (1975).
[10]R. Aaron and R. D. Amado, Phys. Rev. D 13, 2581 (1976).
[11]D. D. Brayshaw, Phys. Rev. Lett. 36, 73 (1976).
[12]R. Aaron, R. D. Amado, and T. Takahashi, Phys. Rev. C 13, 1810 (1976).
[13]G. Gustafson and C. Petersen, Nucl. Phys. B116, 301 (1976).
[14]A. M. Badalyan and Yu. A. Simonov, Institute of Theoretical and Experimental Physics, Moscow, Report No. ITEP-65 (unpublished).
[15]I. J. R. Aitchison, University of Oxford, Department of Theoretical Physics Report No. 58/76 (unpublished).
[16]R. S. Longacre and R. Aaron, Phys. Rev. Lett. 38, 1509 (1977).
[17]G. Mennessier, J.-Y. Pasquier, and R. Pasquier, Phys. Rev. D 6, 1351 (1972). We have avoided the unlikely type-I and type-III two-body parametrizations used in this reference. Our results are qualitatively similar to their type-II parametrization results.
[18]R. Aaron, R. D. Amado, and J. E. Young, Phys. Rev. 174, 2022 (1968).
[19]G. F. Chew and S. Mandelstam, Phys. Rev. 119, 467 (1960).
[20]J. H. Hetherington and L. H. Schick, Phys. Rev. 134, B935 (1965); 139, B1164 (1965); 141, 1315 (1966).
[21]I. M. Barbour and R. L. Schult, Phys. Rev. 155, 1712 (1967).